J. Phys. Chem. A **2001,** *105,* 5081−5095

Impulsive Control of Ground Surface Dynamics of I_3^- in Solution

Erez Gershgoren,[†] **J. Vala,**[‡] **R. Kosloff,**[‡] **and S. Ruhman***[,†]

Institute of Chemistry, The Hebrew University, Jerusalem, 91904 Israel

Received: October 25, 2000; In Final Form: February 14, 2001

Coherent control of I_3^- ground state dynamics in ethanol and acetonitrile solutions is demonstrated. The method is based on impulsive excitation creating a dynamic hole employing sub 30 fsec tunable UV laser pulses. The target of control was to increase the ratio of second to first harmonic spectral modulations of the symmetric stretching vibrational coherences. Methods demonstrated to achieve this target include altering pulse intensity when the excitation pulses are tuned to the maximum of the absorption peak, double excitation pulses separated by half a vibrational cycle, and tuning the pumping or probing pulses to a wavelength simultaneously resonant with both absorption bands of ground state I_3^-. Chirping the probing pulses further allows full mapping of the ground state coherence in phase space, pinpointing the position of the dynamic holes not only in coordinate space but also in momentum. A theoretical model reconstructs the results nearly quantitatively and provides insight into the mechanisms active in achieving the control aims. It further demonstrates how the fundamental suppression serves to precisely characterize the relaxation dynamics of weak spectral features such as higher harmonics of the symmetric stretching and the antisymmetric stretching fundamental. In particular, the ratio of dephasing rates of the first two harmonics (∼2.3) deviates considerably from the ratio of 4 predicted by Kubo line shape theory. Possible sources of this discrepancy based upon alternative dephasing models are discussed.

I. Introduction

Impulsive photoexcitation is a key tool in modern applications of ultrafast spectroscopy to chemical dynamics.[1] It involves optical excitation of molecular species with laser pulses shorter than the time required for the constituent nuclei to move significantly in response to the suddenly modified forces acting between them. A major result of such optical transitions is the nearly vertical promotion of localized material wave packets onto the excited potential surface. The subsequent evolution of this density, probed with a pulse of similar duration, serves to fully reveal the chronology of the excited ensemble, from the initial ground-state geometry to the final products.[2]

An equally important and ubiquitous consequence of impulsive excitation is the buildup of ground-state vibrational coherences. After their generation, the evolution of these coherences gives rise to spectral modulations in the ground-state absorption bands and can be followed as before, with delayed ultrafast probing pulses.[1,3−11] No matter whether this spectroscopic feature is a nuisance, masking a dynamical process of interest, or the main object of the experiment, it is essential to understand its fundamental nature and omnipresence by probing its origins and its dependence upon the experimental parameters.

Initial theoretical descriptions of resonant impulsively induced ground state coherence utilized perturbative expansions of the molecular density matrix, which associated the phenomenon exclusively with the Raman excitation term. This led to its acronym: resonant impulsive stimulated Raman scattering (RISRS).[3,7,9] The analysis showed that from the time evolution of the RISRS spectral modulations, information concerning the underlying vibrational dynamics could be attained which is akin to the constants obtained from frequency domain Raman spectra. The above holds true also for the theoretical analysis of the RISRS process when cast in the dynamically motivated but otherwise equivalent correlation function formalism.[7]

Subsequently, more rigorous approaches to describing the RISRS process were introduced.[12−14] This included work of our own groups,[5,10,11,15] which was dedicated to rationalizing results of a femtosecond laser study of triiodide photodissociation dynamics.[15−19] On the basis of direct integration of the quantum dynamics which explicitly includes the radiation in the Hamiltonian, the material density could be followed directly beyond the range of validity of perturbation theory. When nuclear inertia prohibits substantial motion during the optical pumping, it is justifiable to think of the transition dipole as acting locally in coordinate space. Accordingly, a phase space description of the material density has real advantages over an eigenstate description. Using this approach, an intuitive understanding of the RISRS process can be formulated.[10]

The pump pulse acts to transfer density to the excited potential in a coordinate selective fashion, acting most effectively for the molecular configuration where the potential gap matches the frequency of the light. Thus, if the Bohr frequency is a strong function of the molecular geometry, the field will drill a localized coherent hole in the ground state density. This hole then evolves, giving rise to the spectral modulations from which, when followed by delayed probe pulses, the vibrational dynamics is deduced. The conceptual framework also explains the fine balancing of pulse duration required for optimizing the RISRS signal.[10,11,15] An ideal excitation pulse must be short enough to fulfill the requirements of impulsivity, yet not be so short that it interacts equally throughout the entire coordinate space, leading to a reduction of the ground-state norm without local erosion of portions of the density.

---

[*] To whom correspondence should be addressed.

[†] Also the Farkas Center for Light-Induced Processes.

[‡] Also the Fritz Haber Research Center for Molecular Dynamics.

10.1021/jp0039518 CCC: $20.00

I_3^- is linear and centrosymmetric in its ground and reactive excited states. Accordingly most of the induced dynamics upon excitation is along the symmetric stretch mode. It exhibits a near UV absorption spectrum which is dominated by two major peaks centered at 34 050 and 27 500 cm^{-1}, which at 300 K are ∼3600 cm^{-1} wide.[20−22] The rapid evolution of the excited population, and the fact that the absorption of the primary photoproducts does not strongly overlap with much of this spectrum, conveniently allows delineation of impulsively induced ground-state vibrational dynamics by pumping and probing in the near UV.

In earlier studies, 70 fs pulses centered at 310 nm were employed both as pump and probe in RISRS experiments on I_3^-. The same spectroscopic tool was also used in a transient fashion to follow vibrational relaxation of nascent I_2^- photoproducts.[18] Vibrational dephasing dynamics of the symmetric stretching motion was determined in various polar solvents and in glass forming liquids at reduced temperatures.[19,75] Coherent vibrations were detected only along the symmetric stretch fundamental. No evidence of antisymmetric stretch fundamental activity, known to exist in protic solvents from Raman data,[23,24,70,71] or higher vibrational harmonics, were detected. Kuhne and Vöhringer[25] studied the I_3^- system with a higher time resolution, interpreting the results to indicate activity of higher harmonics and antisymmetric band excitation. A shorter pulse also led to the observation of the second harmonic vibrational coherences in I_2.[26]

The theoretical model was also employed to gain additional insights into the process of impulsively induced ground-state vibronic coherence. The purpose was to set guidelines on how experimental control parameters such as pulse intensity,[11] wavelength, and linear chirp[27−29] influence the induced dynamics and their detection. In the present study, the same molecular system is revisited with improved theoretical tools and with a laser source capable of testing theoretical predictions which exceeded our earlier experimental capabilities. The tunable laser source producing ∼30 fs pulses approaches the impulsive limit to a much greater extent and allows observation of vibration coherence in higher frequency modes.

With these sharper tools for experiment and analysis, the objectives of the present study could be recast in the framework of impulsive coherent control.[30] The pump pulse parameters constitute control levers which can be used to selectively sculpt the ground state density. In an analogous fashion, the parameters of the probe pulse serve as selective filters for observing the transient ground state evolution. These parameters include central wavelength, intensity, relative timing, and residual chirp. The objective of the current study is to investigate the degrees of control afforded by these levers over the RISRS process. Through these insights, manipulation of the pump and probe stages will be used to selectively observe specific modes of vibrational motion and follow their evolution at will.

In this paper, nearly quantitative agreement between the model and experiment is demonstrated. Results show that even at very moderate excitation intensities the observed behavior deviates from the range of validity of perturbation theory. Proper selection of pump and probe pulse wavelengths provides an effective suppression of the symmetric stretch fundamental in the RISRS signal, allowing measurement of the first and second harmonic dephasing dynamics and of antisymmetric stretching activity with enhanced precision. Finally, control of the probe pulse chirp was demonstrated to have strong impact on the RISRS spectral signature, serving to fully map motion of the dynamical hole in phase space.

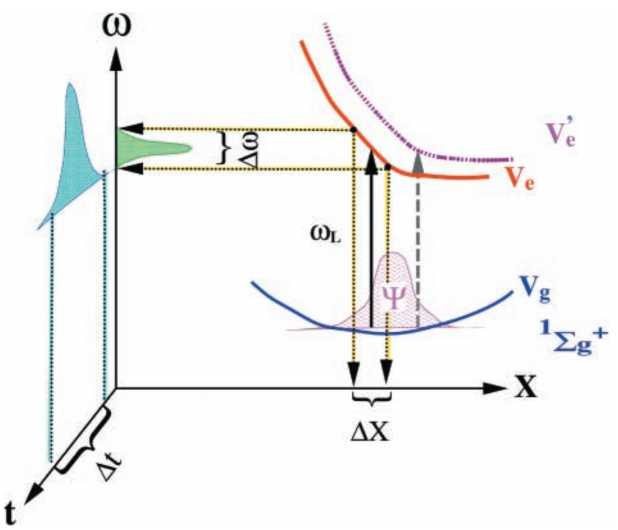

Figure 1. Schematic illustration of the impulsive excitation of the symmetric stretch mode. The pulse shape in the time domain is transformed into a bandwidth in the frequency domain. The coordinate range ΔX influenced by the pulse is obtained by the reflection principle. Notice that for I_3^- there are two excited surfaces V_e and V_e' leading to two overlapping absorption bands.

II. Theory

A theoretical framework of understanding is the basis for interpreting and guiding the experimental studies. This task is achieved by a two tier approach: combining approximate analytic formulas with more rigorous quantum simulation methods. Much of the theory has been developed and tested in previous studies.[10,11,15] The present account briefly reviews the main conceptual points and the simulation methods. The subsection describing the absorption of probe pulse contains new results and, therefore, is described in more detail.

A. Impulsive Control: Coordinate Dependent Two-Level Picture. The conceptual framework of controlling the ground surface dynamics is based on abruptly sculpting the nuclear distribution in phase space. A pulsed optical transition from the ground to the excited electronic surface changes the ground state from a stationary to a nonstationary distribution. The main control knobs on the process are the central excitation frequency ω_L, pulse duration τ_{pump}, amplitude ϵ, and chirp. A more complex control scheme involves a multipulse excitation procedure where the time delay τ_{12} between pulses is an additional control parameter.

In the impulsive limit, a time scale separation exists between the electronic excitation process and the nuclear dynamics. Conceptually the theory resembles the Born−Oppenheimer approximation. Freezing of the nuclear motion during the pulse enables study of the excitation process at each nuclear configuration separately. This is the basis of the coordinate dependent two-level-system approximation.[10,15] For each internuclear configuration X, a local Rabi frequency can be defined:

$$\hat{\Omega}(X) = \sqrt{\hat{\mathbf{\Delta}}^2(X) + \hat{U}^2(X)} \qquad (2.1)$$

where $2\hat{\mathbf{\Delta}}(X) = \hat{\mathbf{V}}_e(X) - \hat{\mathbf{V}}_g(X) - \hbar\omega_L$ is the local RWA detuning and $U(X)$ is the local coupling

$$\hat{U}(X) = \epsilon(X)\cdot\hat{\mu}(X) \qquad (2.2)$$

$\epsilon(X)$ is the instantaneous pulse amplitude mapped onto the coordinate using the reflection principle (Cf. Figure 1) and $\mu(X)$

is the dipole function. The maximum degree of Rabi cycling is determined by the angle $\theta(X)$ defined by $\cos(\theta(X)) = \Delta(X)/\Omega(X)$.

The position dependent Rabi frequency, eq 2.1, is the key to understand the control possibilities. For regions of configuration close to the resonance point X_L, $\Delta(X_L) \ll U(X_L)$ which results in $\theta \approx 90°$. The population can therefore fully cycle between the ground and excited electronic surfaces. The degree of cycling depends on the area under the pulse profile. For pulse intensities less than $\int U(X_L)\,dt = \pi$, the population transferred to the excited electronic surface leaves a void in the ground surface position distribution. The position of the void or dynamical hole can be controlled by tuning the carrier laser frequency ω_L. For pulse intensities larger than π, because of Rabi cycling, the void starts to refill. In the extreme case of a 2π pulse, the void at X_L completely refills. Because of different rates of cycling because $\Omega = \Omega(X)$, each internuclear position obtains a different phase from the field, shifting the final phase space distribution in the momentum direction. Far from the resonance point $\Delta(X) \gg U(X)$, the degree of cycling is small, and therefore, almost no population transfer takes place. The large Rabi frequency results only in a small momentum shift to the initial distribution.[10,13]

Chirping the excitation pulse has two main consequences. First, the chirp has a tendency to correlate the changes in the position and momentum distribution.[27,31,32] Second, at high intensity, the chirp leads to adiabatic transfer.[33,34] The first effect can be understood semiclassically as an excitation that follows the motion of a wave packet. To synchronize with positive momentum, the pulse has to have a negative chirp (from blue to red). A positive chirp will synchronize with the motion of a wave packet with negative momentum. At high intensity, the chirp has an additional effect which leads to adiabatic transfer.[33−35] If the chirp rate is slow relative to the Rabi period, adiabatic transfer prevails and all of the population is transferred from the ground to the excited surface at the particular range of position ΔX. As a consequence, the Rabi cycling is eliminated.[36] Electronic dephasing has a profound effect on the shape of the dynamical "hole". The effect diminishes the population transfer and diffuses the localization of the hole.[10]

B. Simulation. The creation of the dynamical hole was simulated by solving the multisurface time dependent Schrödinger equation for each initial vibrational eigenvalue:

$$i\hbar \frac{\partial}{\partial t}\begin{pmatrix}\tilde{\psi}_e \\ \tilde{\psi}_g\end{pmatrix} = \tilde{\mathbf{H}}\begin{pmatrix}\tilde{\psi}_e \\ \tilde{\psi}_g\end{pmatrix} \tag{2.3}$$

The dynamics were generated by an effective Hamiltonian operator using the rotating wave approximation:

$$\tilde{\mathbf{H}} = \begin{pmatrix}\tilde{\mathbf{H}}_e - \hbar\omega_L/2 & -\bar{\epsilon}(t)\hat{\mu}/2 \\ -\bar{\epsilon}(t)\hat{\mu}/2 & \tilde{\mathbf{H}}_g + \hbar\omega_L/2\end{pmatrix} \tag{2.4}$$

where $-\bar{\epsilon}(t)$ is the envelope of the pump field. Extension to multiple excited electronic states is straightforward. The rotation vector $|\tilde{\psi}\rangle$ is related to the original state by the transformation: $|\tilde{\psi}\rangle = \exp(i\omega_L t\hat{\mathbf{S}}_z)|\psi\rangle$, where $\hat{\mathbf{S}}_z$ is a rotation generator. Propagation in time was performed using a Chebychev polynomial expansion of the evolution operator.[37] The propagation was realized in discrete steps with a time increment shorter by two-orders of magnitude than the pulse duration. The results of the propagation for each initial vibrational wave function were combined with Boltzmann weights to construct the final state: $\hat{\rho}_f = \Sigma_i e^{-\beta \mathbf{E}_i}|\psi_i(t_f)\rangle\langle\psi_i(t_f)|$ where $\psi_i(t_f)$ is the wave function on the ground surface after the pulse is over. The projection of $\hat{\rho}_f$ on the ground surface was the starting point of simulations including the dissipative dynamics, on the basis of propagating the Liouville von Neumann equation.[15]

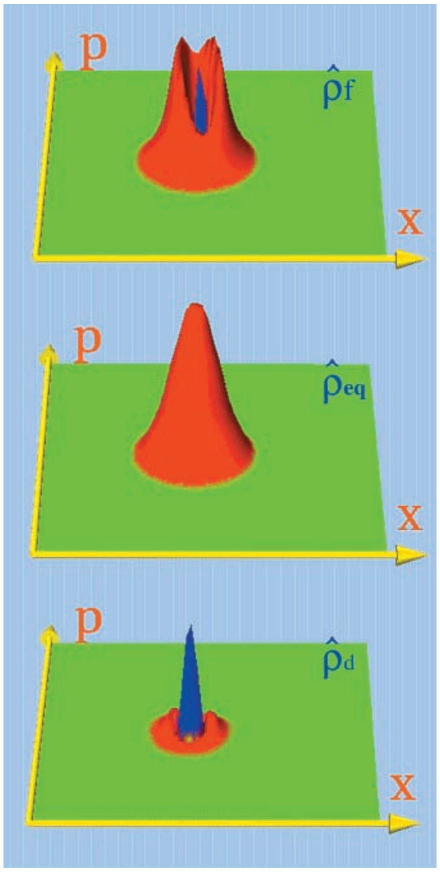

Figure 2. Phase space picture of the state created by the pump pulse $\hat{\rho}_f$ is shown in the upper panel. Below, the initial state $\hat{\rho}_{eq}$ and the dynamical hole $\hat{\rho}_d = \hat{\rho}_f - c^2\hat{\rho}_{eq}$ are also shown. In this example, the hole is created by an excitation pulse with a frequency corresponding to the center of the lower absorption band, i.e., 364 nm. The states are shown as Wigner functions in phase space in scalled coordinates, where blue color represents negative density (see text).

The detected signal is proportional only to the dynamical part of the ground surface density. This leads to a definition of the dynamical hole which is orthogonal to the equilibrium state:[10] $\hat{\rho}_d = \hat{\rho}_f - c^2\hat{\rho}_{eq}$, where $\hat{\rho}_f$ is the density operator after the pulse $\hat{\rho}_{eq}$ is the stationary or initial density operator. c^2 is the normalized scalar product $c^2 = tr\{\hat{\rho}_f \cdot \hat{\rho}_{eq}\}/tr\{\hat{\rho}_{eq}^2\}$, which represents the difference between the final state and the initial equilibrium state. A measure of the coherence induced by the pump has been defined as[10] $C^2 = tr\{\hat{\rho}_d^2\}$, which equally represents the depth of the dynamical hole.

A Wigner function[38,39] of the final density operator

$$W_f(p,x) = \frac{1}{2\pi}\int \hat{\rho}_f(x - y/2,\, x + y/2)e^{ipy}\,dy \tag{2.5}$$

as well as one for the hole $W_d(p,x)$ were generated for visualizing the state prepared by the pump pulse. Figure 2 shows the Wigner function created in this fashion using scalled position and momentum coordinates $\bar{x} = (m\omega/\hbar)^{1/2}x$ and $\bar{p} = (1/m\omega\hbar)^{1/2}p$. In these coordinates, the unitary time evolution is simply a rotation around the origin in phase space.

The negative density in the Wigner function of $\hat{\rho}_f$ (the blue color in the upper panel) is evidence for a purely quantum mechanical contribution to the distribution in phase space reflecting interference in the light-induced coherent motion.

C. Absorption of the Probe Pulse. The total energy absorbed by the probe pulse is linearly related to the change in population on the ground electronic surface[15]

$$\Delta E = -\hbar\omega_{\mathrm{L}}\Delta N_{\mathrm{g}} \tag{2.6}$$

The change in population ΔN_{g} can be simulated directly by solving eq 2.3 with the characteristics of the probe pulse. The initial condition is the transient wave function induced by the pump on the ground electronic surface. It is assumed that the excited part of the wave packet at the probing time t_{p} has already dissociated and thus moved out of the observation window.

An approximate alternative to the direct simulation of the probe signal is obtained by an observable represented by a window operator $\hat{\mathbf{W}}$:

$$\Delta E \approx -\hbar\omega_{\mathrm{L}} tr\{\hat{\rho}(t_{\mathrm{p}})\cdot\hat{\mathbf{W}}\} \tag{2.7}$$

The window operator provides direct insight into the probing process as well as reducing the computational effort. Equation 2.7 implies that the window operator $\hat{\mathbf{W}}$ is independent of the state of the system $\hat{\rho}(t_{\mathrm{p}})$. This statement is true if the intensity of the probe pulse vanishes, which eliminates the contribution of cycling back from the excited electronic surface. Moreover, the observation process is not instantaneous and is completed in a time duration proportional to the probe pulse duration τ_{p}. The concept of eq (2.7) is to collapse the observation to a single instant of time t_{p}. The collapse assumption for the window operator is equivalent to the impulsive condition that the nuclear motion is frozen during the observation.

Because the static contribution is subtracted from the signal, the probe signal observation can also be viewed as an overlay between the density of the hole W_{d} in phase space and a compact Wigner-Weyl function[38,39] $W_{\mathrm{w}}(p,x) = 1/(2\pi)\int \hat{\mathbf{W}}(x - y/2, x + y/2)e^{ipy}\,dy$, representing the observation window:

$$\mathrm{Signal} = \Delta E \approx -\hbar\omega_{\mathrm{L}}\int\int \mathrm{d}p\,\mathrm{d}x\,W_{\mathrm{d}}(p,x)W_{\mathrm{w}}(p,x) \tag{2.8}$$

Equation 2.8 is the basis of the conceptual insight on the emergence of the transient signal form the overlap in phase space between the dynamical hole and the window operator.

Explicit expressions of the window operator are obtained by considering an initial state on the ground electronic surface $\psi_{\mathrm{g}}(t_{\mathrm{p}} - c\tau_{\mathrm{p}})$ at a time $c\tau_{\mathrm{p}}$ before the probing time t_{p}. The constant c is determined such that $\epsilon(t \pm c\tau_{\mathrm{p}}) \approx 0$. This initial state will evolve under the influence of the probe pulse to

$$\begin{pmatrix} 0 \\ \psi_{\mathrm{g}}(t_{\mathrm{p}} - c\tau_{\mathrm{p}}) \end{pmatrix} \rightarrow \begin{pmatrix} \psi_{\mathrm{e}}(t_{\mathrm{p}} + c\tau_{\mathrm{p}}) \\ \psi_{\mathrm{g}}(t_{\mathrm{p}} + c\tau_{\mathrm{p}}) \end{pmatrix} \tag{2.9}$$

Because of the total norm conservation, the change in norm on the ground surface can be measured on the excited surface:

$$\Delta N_{\mathrm{g}} = -\Delta N_{\mathrm{e}} = -\langle\psi_{\mathrm{e}}(t_{\mathrm{p}} + c\tau_{\mathrm{p}})|\psi_{\mathrm{e}}(t_{\mathrm{p}} + c\tau_{\mathrm{p}})\rangle$$

For a probe which typically has weak intensity, time dependent perturbation theory can be used to obtain the final excited-state wave function $\psi_{\mathrm{e}}(t_{\mathrm{p}} + c\tau_{\mathrm{p}})$ from the initial ground-state wave function $\psi_{\mathrm{g}}(t_{\mathrm{p}} - c\tau_{\mathrm{p}})$:

$$|\psi_{\mathrm{e}}(t_{\mathrm{p}} + c\tau_{\mathrm{p}})\rangle = \frac{i}{\hbar}\int_{-c\tau_{\mathrm{p}}}^{+c\tau_{\mathrm{p}}} \mathrm{d}\tau\,\exp[-i/\hbar\hat{\mathbf{H}}_{\mathrm{e}}(c\tau_{\mathrm{p}}-\tau)]\hat{\mu}\epsilon^*(\tau) \\ \exp[-i/\hbar\hat{\mathbf{H}}_{\mathrm{g}}(\tau+c\tau_{\mathrm{p}})]|\psi_{\mathrm{g}}(t_{\mathrm{p}} - c\tau_{\mathrm{p}})\rangle \tag{2.10}$$

Under the impulsive conditions $[\hat{\mathbf{H}}_{\mathrm{e}}, \hat{\mathbf{H}}_{\mathrm{g}}] \approx 0$, eq 2.10 simplifies to

$$|\psi_{\mathrm{e}}(t_{\mathrm{p}} + c\tau_{\mathrm{p}})\rangle = \\ \exp(-i/\hbar\hat{\mathbf{H}}_{\mathrm{e}}c\tau_{\mathrm{p}})\left\{\frac{i}{\hbar}\int_{t_{\mathrm{p}}-c\tau_{\mathrm{p}}}^{t_{\mathrm{p}}+c\tau_{\mathrm{p}}} \mathrm{d}\tau\,\exp(-i/\hbar 2\hat{\mathbf{\Delta}}\tau)\hat{\mu}\bar{\epsilon}^*(\tau)\right\} \\ \exp(-i/\hbar\hat{\mathbf{H}}_{\mathrm{g}}c\tau_{\mathrm{p}})|\psi_{\mathrm{g}}(t_{\mathrm{p}} - c\tau_{\mathrm{p}})\rangle \tag{2.11}$$

where $\epsilon(t) = \bar{\epsilon}(t)\exp(i\omega_{\mathrm{L}}t)$. The structure of eq 2.11 allows a synchronization of the ground and excited wave function to a common time t_{p}, leading to

$$|\psi_{\mathrm{e}}(t_{\mathrm{p}})\rangle = \left\{\frac{i}{\hbar}\int_{t_{\mathrm{p}}-c\tau_{\mathrm{p}}}^{t_{\mathrm{p}}+c\tau_{\mathrm{p}}} \mathrm{d}\tau\,\exp(-i/\hbar 2\hat{\mathbf{\Delta}}\tau)\hat{\mu}\bar{\epsilon}^*(\tau)\right\}|\psi_{\mathrm{g}}(t_{\mathrm{p}})\rangle \tag{2.12}$$

Equation 2.12 relates any arbitrary initial wave function on the ground surface to the final wave function on the excited surface, collapsed to a single instant of time. The window operator is therefore constructed from the projection composed from the curly bracket in eq 2.12.

For a Gaussian shaped probe pulse with the envelope function, $\bar{\epsilon}(t) = Ae^{-(t-t_{\mathrm{p}})^2/2\tau_{\mathrm{p}}^2}$, eq 2.12 can be integrated leading to the window operator:

$$\hat{\mathbf{W}}(x,x') = \frac{\pi(\tau_{\mathrm{p}}A)^2}{\hbar^2}\exp\left(\frac{-2\Delta^2(x)}{\hbar^2}\tau_{\mathrm{p}}^2\right)\cdot\hat{\mu}^2(x)\delta(x - x') \tag{2.13}$$

This expression is identical to the one obtained by Ungar and Cina.[14] A similar expression can be obtained for a square pulse where the Gaussian is replaced by a sinc function.[15]

The window operator representing the probe absorption signal can be interpreted as a finite precision position measurement performed on the ground surface density $\hat{\rho}_{\mathrm{g}}$. The precision of the position measurement is determined by the slope of the difference potential $2\Delta(x)$, at the point of resonance: $\alpha = 2\,\mathrm{d}\Delta(x)/\mathrm{d}x|_{\Delta=0}$, leading to $\Delta X \approx \hbar/\alpha\tau_{\mathrm{p}}$ (see Figure 1). For the I_3^- system, with a pulse duration of $\tau_{\mathrm{p}} = 25$ fs, the resolution in position in the symmetric stretch direction becomes $\Delta X = 0.1$ Å.

Chirping the probe pulse modifies the window operator. Consider the following chirped pulse:

$$\epsilon(t) = A\exp\left[\frac{-(t - t_{\mathrm{p}})^2}{2\tau_{\mathrm{p}}^2} + i\frac{\chi}{2}(t - t_{\mathrm{p}})^2 + i\omega_{\mathrm{L}}(t - t_{\mathrm{p}})\right] \tag{2.14}$$

where χ measures the chirp rate. Because the chirp lengthens the pulse, the impulsive approximation is corrected by the next order in τ in the exponent of eq 2.10, i.e., $[\hat{\mathbf{H}}_{\mathrm{e}},\hat{\mathbf{H}}_{\mathrm{g}}] = 2[\hat{\mathbf{\Delta}},\hat{\mathbf{P}}^2/2M] \approx i\hbar\alpha\hat{\mathbf{P}}/M$. This will lead to the following excited-state wave function:

$$|\psi_{\mathrm{e}}(t_{\mathrm{p}})\rangle = \left\{\frac{i}{\hbar}\int_{-c\tau_{\mathrm{p}}}^{+c\tau_{\mathrm{p}}} \mathrm{d}\tau\,\exp\left[-\frac{i}{\hbar}2\hat{\mathbf{\Delta}}\tau - \frac{\tau^2}{2\tau_{\mathrm{p}}^2}\right] \\ \exp[i(\chi/2 - \alpha/2\hbar\,\hat{\mathbf{P}}/\mathrm{M})\tau^2]\hat{\mu}\right\}|\psi_{\mathrm{g}}(t_{\mathrm{p}})\rangle \tag{2.15}$$

Comparing eq 2.15 to eq 2.12, one finds that the chirp rate χ is correlated with the velocity $\bar{v} = \langle\hat{\mathbf{P}}/M\rangle$. On performing the integration, the window operator is approximated as

$$\hat{\mathbf{W}}(x,x') \propto \exp\left[-\frac{2\Delta^2(x)}{\hbar^2}\tau_{\mathrm{p}}^2\frac{2}{1 + \tau_{\mathrm{p}}^4(\chi/2 - (\alpha/2\hbar)\bar{v})^2}\right]\cdot \\ \hat{\mu}^2(x)\,\delta(x - x') \tag{2.16}$$

The window operator in eq 2.16 enhances areas in phase space where the velocity is correlated with the chirp rate. Taking the

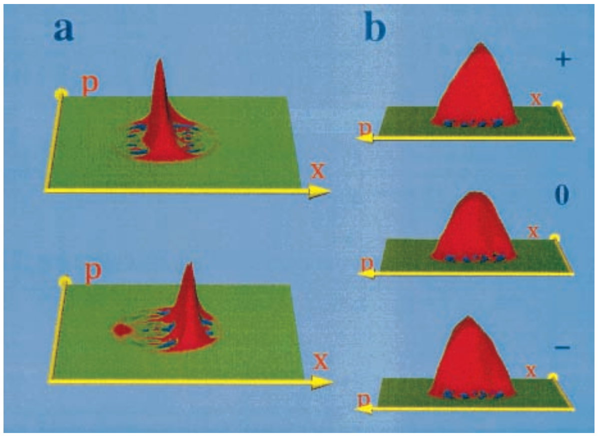

Figure 3. Window operator in phase space. (a) Top: a probe centered at 364 nm. Bottom: a probe centered at 400 nm. (b) The influence of the chirp on a window function centered at 400 nm. The ± signs represent the positive and negative chirp of 500 fs^2. Notice that the phase space in panel b is rotated by 90° with respect to panel a.

next order in the expansion of Δ, i.e., $\alpha_2 = (d^2\Delta/dx^2)_{\Delta=0}$, through the commutator of the ground and excited Hamiltonian will add the momentum position correlation operator $i\hbar\alpha_2/M$ $(\hat{\mathbf{X}}\hat{\mathbf{P}} + \hat{\mathbf{P}}\hat{\mathbf{X}})$ to eq 2.16. This addition will cause a rotation in phase space of the window operator (see section IV.D). The present approach to a chirped probe is different than the semiclassical approach of Zadoyan et al.[32] where the window function is defined only in coordinate space.

The concept of synchronizing the ground and excited wave functions to a common time t_p can be used to obtain a numerical representation of the window operator. Each initial eigenfunction ϕ_n on the ground electronic surface at time $t = -c\tau_p$ evolves to an excited-state wave function $\psi_e(n)(+c\tau_p)$, where the peak of the probe intensity is shifted to time $t = 0$. These wave packets are propagated backward in time under the free evolution on the excited surface to $t = 0$: $\psi_e(n)(0) = e^{+i/\hbar\hat{\mathbf{H}}_e c\tau_p}\phi_e(n)(+c\tau_p)$. The window operator is constructed from the sum of excited-state projections from all of the initial eigenvalues. To complete the synchronization, the window operator is propagated forward in time for duration $c\tau_p$ generated by free evolution on the ground surface Hamiltonian:

$$\hat{\mathbf{W}} = -\exp[-i/\hbar\hat{\mathbf{H}}_g c\tau_p](\sum_n |\psi_e(n)(0)\rangle\langle\psi_e(n)(0)|) \exp[+i/\hbar\hat{\mathbf{H}}_g c\tau_p] \quad (2.17)$$

The window operators are shown in phase space in Figure 3.

The blue color regions representing negative density are an indication of the failure of the perturbation description, eq 2.15, even for vanishingly small probe intensities. The basic assumption in the perturbative expansion is that population moves unidirectionally from the ground to the excited surface or in a two-level description the light induces only a small fraction of a Rabi cycle. However, the Rabi frequency for vanishing intensity, $\Omega(X) \approx |\Delta(X)|$, is proportional to the detuning. Therefore, even for zero intensity for large detuning, there is considerable cycling. These considerations define the range of validity of the perturbation approach as $\Delta(X)\cdot\tau_p \ll \hbar$. For a pulse of 30 fs for the I_3^- system, this translates to a detuning of $\Delta(X) \ll 1500\ cm^{-1}$.

III. Experimental Procedures

A. Experimental Details. The amplified laser used in this study removes two major limitations imposed by its predecessor: mediocre time resolution and the inability to tune the excitation pulses. The current homemade system provides a high repetition rate source of nearly transform limited pulses which are continuously tunable from the near-IR to the UV. The system consists of a KLM Ti;sapphire oscillator and multipass amplifier, coupled to a commercial OPA (TOPAS, Light Conversion). The oscillator follows the design published by Asaki et al.[40] and is pumped with 4 W of argon ion radiation (Coherent Innova 310). This oscillator, which was built around a crystal purchased from EKSMA, produces a 300 mW train of 17 fs pulses, with a FWHM spectral band of 45 nm, and an 85 MHz repetition rate. Before amplification, the pulses were stretched in an all reflective stretcher, which preserves the spectral width of the oscillator output, to a duration of 25 ps. The stretcher was constructed from a 600 line/mm grating (Richardson Grating Lab) and a 6 in. gold parabolic mirror of 91 cm focal length (Edmund Scientific).

After a single pulse was selected from the stretched pulse train at a frequency of 1 kHz (Pockells cell; Fast Pulse Technology), the pulse was injected into a multipass amplifier pumped with 10 mJ pulses from an intracavity doubled YLF laser (527 Quantronix DP-H). The amplifier is based on the design of Backus et al.,[41] with some modifications. Pumping was achieved axially by focusing the YLF output into a 6 mm optical path length brewster cut sapphire crystal (Casix). This is achieved using 2 in. diameter dichroic end mirrors with 75 cm radii of curvature (CVI), which transmit the pumping radiation and reflect the near-IR. A mask of 2.2 mm holes on 3.6 mm centers is introduced between the planar gold reflector and one of the end mirrors to reduce effects of ASE, and self-focusing. 8 round trips in the amplifier produce a 1.3 mJ pulse (13% conversion of the pump energy). The amplified pulses were spatially filtered and temporally compressed with a grating pair to produce the ultimate output of 28 fs (FWHM) pulses containing 700 μJ of energy, at 1 kHz. The spectrum of the output is centered at 800 nm. 80% of this output is used to pump the OPA, generating 18−22 fs pulses throughout the visible range (450−750 nm) via frequency doubling the IR output or nonlinear mixing with the 800 nm fundamental.

The UV pulses were generated by quadrupling the OPA output in sub-100 micron BBO crystals which minimize pulse broadening because of group velocity mismatch. Prism pairs were used to control linear chirp both before and after the BBO doubling crystals, to obtain the highest time resolution. In some experiments linear chirp was intentionally introduced by increasing or decreasing the depth of prism insertion in the same compensating pairs.

I_3^- solutions were prepared by mixing iodine and iodide salt (KI for ethanol or $(CH_3)_4NI$ for acetonitrile) with a 10% excess of iodide. The concentration of the solution changed from experiment to experiment to provide 50% absorption of pump energy. The integrity of the solution was monitored by measuring the UV−vis absorption spectrum before and after the experiments, and demonstrated to be unchanged by the irradiation. The sample was circulated through a 200 μm path length cell equipped with 150 μm quartz windows, using an all Teflon peristaltic pump (Cole Parmer), at a rate which refreshed the sample irradiated between shots.

Pump and probe pulses were focused through a 25 cm quartz singlet into the sample. Intensity of the pump and probe pulses, as well as the transmitted probe, were collected by amplified photodiodes and digitized on a fast A/D converter. The transmitted probe was subtracted from the reference pulse in a lock-in amplifier (EG&G, 7260) and the pump beam chopped at 500 Hz. The resulting signal detected at this frequency was digitized and dynamically normalized to changes in pump and probe reference intensities. The time delay between pump and probe was controlled by a high-resolution DC motor actuated translation stage (Newport, PM500). Computer control of the data collection as well as the subsequent data analysis to be described below were programmed in Labview.[42]

B. Experimental Analysis. The outcome of the experiment was a time series, composed of the absorption of the probe pulse at incremental time delays: $S_{\mathrm{ex}}(n\Delta t)$. The time series reflects the ground-state nuclear motions induced by the pump and viewed by the probe. The ultimate goal of the analysis is a breakup of the spectral modulations into contributions from individual active vibrational modes and to extract accurate values for their frequencies and decay dynamics.

A powerful tool employed for this purpose is the filter diagonalization technique.[43−45] The method is based on the assumption that the time signal can be represented as a sum of complex exponentials:

$$S(t) = \sum_{j=1}^{K} d_j \exp(-i\omega_j t) \tag{3.1}$$

where $\Omega_j = \mathrm{Re}(\omega_j)$ is the desired frequency, $\tau_j = 1/Im(\omega_j)$ is the life time, and d_j is the complex amplitude of the jth component. $4K$ is the number of fitting parameters. The assumption of exponential vibrational dephasing of each component is by no means assured in view of contrary examples in the literature.[46] Implications of this assumption will be addresses in section V.

The analysis method employs only a small frequency window inside the physically relevant range. In this range, the frequencies are extracted by diagonalization of a small matrix. The matrix elements are evaluated directly from a stroboscopic sampling of the signal $S(n\Delta t)$ where Δt is the sampling interval. The method is particularly suited for pump−probe ultrafast experiments where Δt is determined to a very high precision (± 0.3 fs).

The experimental background of the signal was eliminated either by the subtraction of a low order polynomial fit to the data (order 2−3) or by letting the Filter-Diagonalization procedure fit the background. The relevant frequencies above 100 cm^{-1} were not sensitive to the background subtraction method.

The advantage of the method is the ability to extract the desired parameters, with high fidelity, using only a limited number of data points. The validity of the output parameters was checked in the time and frequency domains. In the time domain, the results were checked by eq 3.1. The experimental signal was reconstructed starting with the frequencies with the largest amplitudes $|d_j|$. For each additional frequency, ω_j that was added to the sum, the signal was compared to the experimental output. When the agreement with the experimental data was satisfactory the procedure was stopped. This constitutes the minimum set of amplitudes and frequencies which reconstruct of the experimental signal. Adding frequencies beyond the minimum set increased χ^2, where $\chi^2 = \sum_{n=1}^{N}(S_{\mathrm{ex}}(n\Delta t) - S(n\,\Delta t))^2/(N - 4K)$. In the frequency domain, the spectrum was reconstructed using the relation

$$F(\omega) = \sum_j \frac{d_j}{\omega - \omega_j} \tag{3.2}$$

The $F(\omega)$ function was reconstructed with the minimum set of frequencies and compared to the Fourier transform of the experimental signal. In the analyzed signals, aside from very rapidly decaying or very low-frequency components, the leading amplitudes could be assigned to the known molecular modes, their harmonics and combination bands.

There were cases where the analysis resulted in a group of close-lying frequencies. The possibility of regrouping these frequencies was checked by using a nonlinear fit procedure to refit the experiment with only one representative frequency. A nonlinear fit procedure was also used to check the possibility of non exponential decay. The χ^2 criteria was used to determine if this procedure was valid.

The filter-diagonalization (FD) fitting procedure can be compared to the linear prediction singular value decomposition (LP-SVD)[47] procedure because both methods fit the data to a similar functional form. The advantage of the FD is that the stroboscopic structure of the data is incorporated in the method. Typically in pump probe spectroscopy the time delay is determined very accurately compared to the amplitude of the signal which is affected by noise. The FD method is ideally suited for such situations.[48]

IV. Case Studies

Once the target of control was defined as suppression of the symmetric stretch fundamental and the enhancement of the remaining frequencies, a number of distinct strategies were studied. Each subsection describes a specific strategy, its experimental implementation, and theoretical foundation.

After the concept of both the dynamical hole and the probing window function are described, the general approach for suppressing the first harmonic component of the symmetrical stretching in the RISRS signal is straightforward. The complete signal cycle involves both the generation of the hole by the pump and its observation through the coordinate dependent mask defined by the probe. We concentrate on a two-dimensional representation of vibrational phase space in terms of the symmetrical stretching mode and disregard the possibility of a chirped probe. All that is required for first harmonic suppression is to prepare a dynamical hole and/or to devise a probe window function with C_2 symmetry in phase space, assuming the rotation axis is perpendicular to the (p,x) plane and centered at its origin. Either or both of these will ensure that one period of phase space rotation (one period of vibration) will produce a signal with two repeated and identical time sections, excluding a first harmonic component at the fundamental frequency by definition. The following case studies will examine specific strategies for obtaining this goal and describe their limitations and fortitudes with respect to the control objective.

A. Drilling a Hole in the Middle of the Absorption Band. By tuning the pump frequency ω_{L} to the center of the absorption band, the dynamical hole in coordinate space is produced with reflection symmetry with respect to the minimum point of the potential well. If inversion symmetry is also imposed with respect to zero momentum, the desired C_2 symmetry is obtained. A momentum kick induced by the pump will break this symmetry leading to the appearance of a first harmonic component in the signal. A measure of the degree of symmetry breaking of the dynamical hole is defined as the momentum change on the ground surface normalized to the depth of the dynamical hole:

$$\bar{P} = \frac{\langle \hat{\mathbf{P}} \rangle}{C} = \frac{tr\{\hat{\mathbf{P}}\hat{\rho}_{\mathrm{d}}\}}{C} \tag{4.1}$$

where C is the coherence measure (cf. subsection II.B).

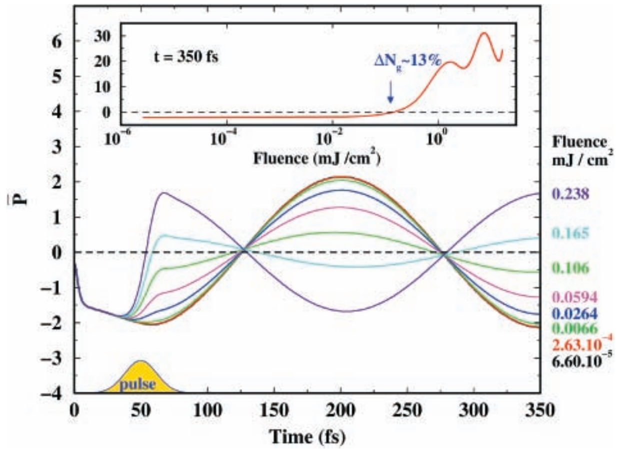

Figure 4. The buildup of the momentum kick $\bar{P}$ as a function of time for different intensities. The duration of the pulse is indicated. After the pulse is over the momentum kick $\bar{P}$ oscillates with the period of the fundamental frequency. The insert shows the final momentum kick $\bar{P}$ determined after the pulse is over as a function of fluence, showing the transition from negative to positive momentum.

The source of the momentum kick is quite subtle. We found by simulation that our previous semiclassical estimations[10,15] were misleading. Figure 4 shows the buildup of the momentum kick during the pulse. At small fractions of the Rabi cycle, i.e., $Ut \ll \pi$, a universal buildup of a negative momentum kick $\bar{P}$ is observed. In this region of intensity, the momentum $\langle \hat{\mathbf{P}} \rangle$, the coherence measure C, and the population transfer ΔN_g all scale linearly with the fluence (ϵ^2). This phenomena can be rationalized by first decomposing the zero momentum initial stationary state to a superposition of pairs of wave packets with positive and negative momentum. The absorption process has a bias to the promotion of the positive momentum wave packet, thus leaving behind a negative momentum contribution. This phenomena is related to the different absorption of a positive or negatively chirped pulse.[27,36] The zero intensity negative momentum kick means that a residual symmetry breaking, causing a first harmonic signal, will occur even at very small fluence values. The broken symmetry in the dynamical hole for low fluence is clearly observed in panel 1 of Figure 5 which shows a phase space picture of the dynamical hole $\hat{\rho}_d$.

Upon increasing intensity the $\bar{P}$ increases nearly linearly with fluence and eventually changes sign (cf. Figure 4). This effect is purely quantal because it results from interference between the ground state wave function and the wave transferred back from the excited state by the optical cycling, see Figure 5. The population transfer which accompanies the change of sign of $\bar{P}$ is moderate $\Delta N_g \sim 13\%$. This point represents a peak ratio in second to first harmonic amplitude. This maximum is clearly observed in the experimental signal (cf. Figure 6). Further increase in intensity was found to reduce this ratio, which is consistent with an increase of the positive momentum kick.

For even higher pump intensities the momentum distribution changes shape almost completely loosing the C_2 symmetry. This is the result of additional interference causing an oscillation in the momentum kick as a function of fluence (cf. Figure 5). Figure 5 confirms the analysis that the C_2 symmetry breaking is in the momentum direction. This fact means that the peak of the first harmonic components will coincide with half the transmission peaks of the second harmonic component. As a result, one of the peaks of the second harmonic component will be enhanced, creating a sawtooth like signal with a different direction for negative and positive momentum kick (cf. Figure 6).

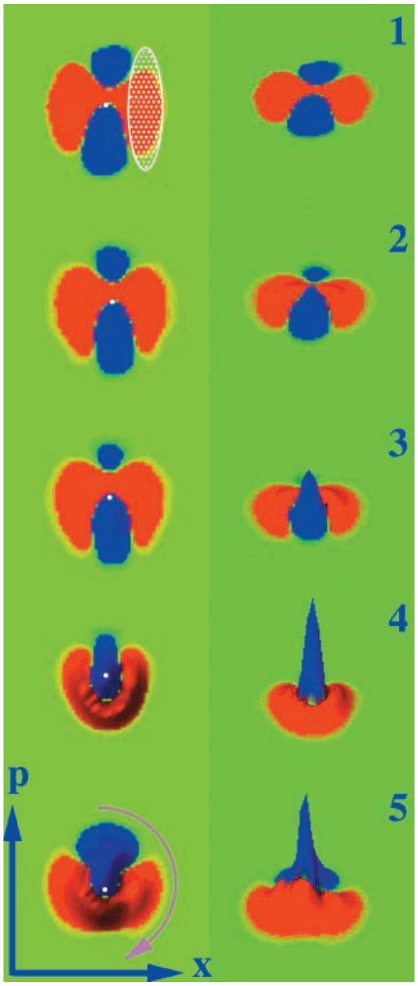

Figure 5. Intensity effect on a hole $\hat{\rho}_d$ drilled in the middle of the band (364 nm) showing the breaking of the C_2 symmetry. The intensities are in units of fluence, where panel 1, 0.017 mJ/cm^2 ($\Delta N_g = 0.02$); panel 2, 0.14 mJ/cm^2 (0.13) $\bar{P} = 0$; panel 3, 0.24 mJ/cm^2 (0.19); panel 4, 0.66 mJ/cm^2 (0.23); panel 5, 2.63 mJ/cm^2 (0.30). The ellipse in panel 1 represents the probe window W_w located at 400 nm. The white point represents the origin of rotation in phase space which is the zero position momentum point. The left panels show a top view, whereas the right panel shows a stereoscopic perspective.

The insight gained by this analysis leads to the possibility of controlling the relative phase between the first and second harmonic components using intensity and detuning as control knobs. A phase shift of $\pi/2$ (with respect to the fundamental frequency) between the first and second harmonic components can be obtained by symmetry breaking in the coordinate direction. This operation is easily obtained by detuning the excitation frequency slightly off the center of the absorption band. A combination of intensity and detuning enables control of the amplitude ratio as well as control of the relative phase of the first and second harmonic components of the signal. Alternatively, observing the transient signal allows a direct determination of the initial shape in phase space of the dynamical hole.

Figure 6 displays the measured pump probe signal for different intensities corresponding to the simulation presented in Figure 5. The transition from a signal with a significant first harmonic component for low intensity to a signal dominated by a second harmonic component at higher intensity and a decrease of the second harmonic component for even higher intensity is evident in the time domain, where the main period of oscillation doubles. This is born out in the spectral analysis

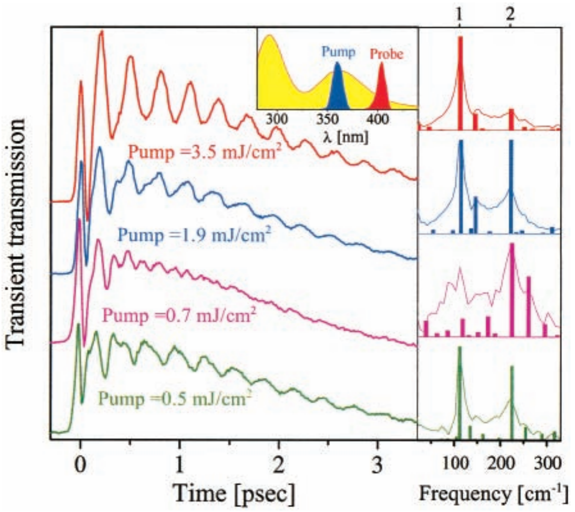

Figure 6. Pump probe signal of I_3^- in ethanol for four different pump intensities. The spectrum of the pump and probe pulses is indicated in the insert superimposed on the absorption spectra of I_3^-. The right panel shows the Fourier transform of the signal together with the filter-diagonalization fit to the data shown as histograms indicating the main frequencies and amplitudes in the data. The top label indicates the position of the fundamental frequency 111 cm^{-1} and its second harmonic. The insert shows the spectrum of the pump and probe pulses superimposed on the absorption spectrum of I_3^-.

shown in the right panel of Figure 6. The other significant frequency in the data is the antisymmetric stretch $\omega = 145$ cm^{-1}, indicating a breaking of symmetry of the I_3^- molecule by the solvent.[23,24,50]

A series of experiments were performed where both the pump and probe were in the middle of the absorption band either at 364/364 or, for the upper band, at 290/290. With a careful selection of the wavelength and chirp, the first harmonic signal was suppressed almost completely because of C_2 symmetry of the probing window function in phase space.

B. Drilling Two Holes Simultaneously. Pump 325 nm Probe 400/325 nm. The absorption spectrum of I_3^- is composed of two overlapping absorption bands. By choosing an excitation frequency where the two absorptions are equal, two holes are created (see Figure 1). Because the two holes are positioned nearly symmetrically around the zero point in phase space, the desired C_2 symmetry is approximately obtained. Panel b in Figure 8 shows the phase space distribution after the pump. The excitation removes amplitude from both sides of the initial distribution, creating a state which is narrower than its uncertainty width in the ground state. Such a nonclassical distribution indicated by its negative components (blue) resembles a "squeezed state" in quantum optics.[51,52] The distribution of the hole shows that a probe far from the center will experience more first harmonic character than a probe close to the center of the absorption band. This is evident in Figure 7, where a probe at 400 nm shows dominant first harmonic dynamics. A probe at 325 nm shows dominant second harmonic dynamics due to a filtering effect of the double probing window. At first sight the pump probe signals in the two solvents look very similar. A more careful examination, in particular by filter-diagonalization analysis, reveals an antisymmetric contribution in I_3^- in ethanol which will be absent from the acetonitrile data.

The 325/325 trace in the acetonitrile data has the typical characteristics of a $\pi/2$ phase shift between the first and second harmonic components. This means that the symmetry breaking is along the momentum direction which could be interpreted as an intensity effect. Other traces with the similar pump probe wavelength combinations (not shown) display a sawtooth like signal indicating symmetry breaking in the coordinate direction.

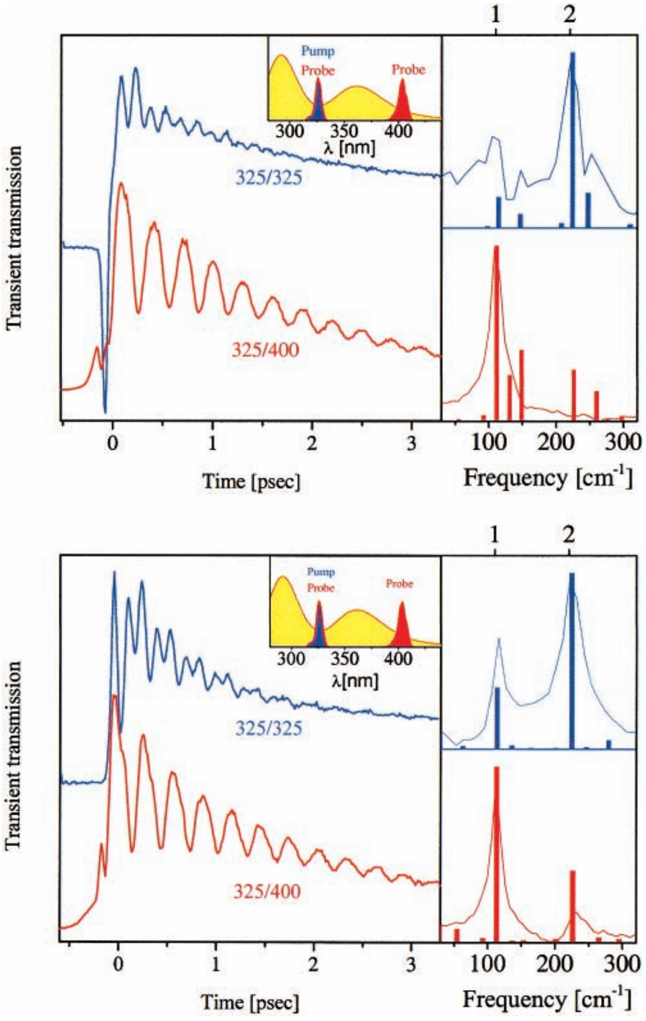

Figure 7. Pump probe signal for I_3^- in ethanol (top) and acetonitrile (bottom). The pump wavelength is at 325 nm. The top trace shows a probe at 325 nm and the bottom trace shows a probe at 400 nm. The right panel displays the filter-diagonalization fit to the dominant frequencies superimposed on the Fourier transform of the data.

C. Multipulse Excitation. Pump 400/400 nm Probe 400 nm. A generally applicable method for ensuring the C_2 symmetry in phase space is the introduction of a double excitation pulse delayed by half a fundamental period. A similar method was previously used for studying interference effects in impulsive Brillouin scattering.[49] The holes created have similarities to the ones created by the simultaneous drilling of two holes.

From an eigenstate viewpoint, the double excitation creates a constructive interference for the even eigenstates and a destructive interference for the odd eigenstates. This process can be observed in Figure 9. As an indication of a coherent process, the amplitude of the $v = 2$ component after the second pulse is enhanced by a factor of ~5 relative to its amplitude after the first pulse.

From the phase space viewpoint, one can imagine the effect of the pulse as first shaving one side of the distribution and then using the dynamics to rotate the distribution by 180° and shaving the other side of the distribution. This effect can also be utilized to make higher order harmonics by using three pulses separated by $^1/_3$ of a period etc. The shape of the dynamical hole created by this method is shown in the top panel of Figure

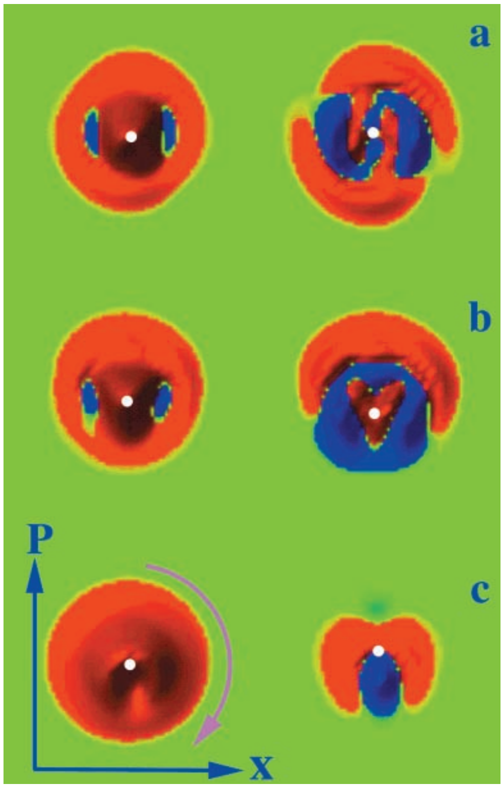

Figure 8. Comparison of final density W_f (left panel) and dynamical density W_d (right panel), created by (a) sequential drilling of two holes by half a period delay (excitation at 400/400 nm) to (b) simultaneous drilling of two holes (excitation at 325 nm) and to (c) an intermediate intensity hole drilled in the center of the band. (excitation at 364 nm).

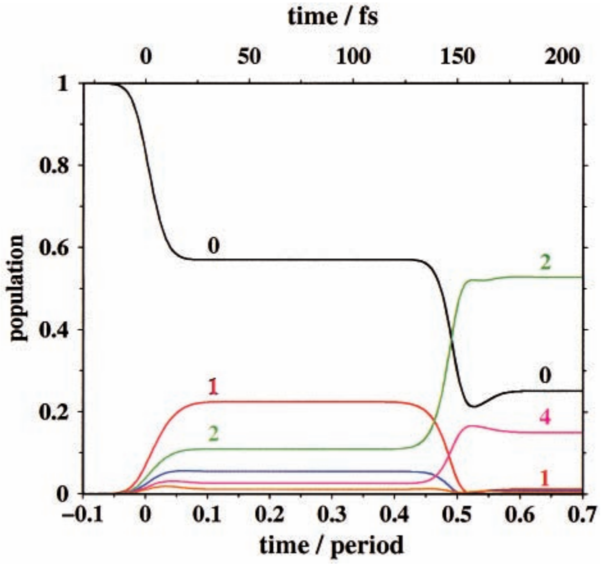

Figure 9. Creation of a hole by a double pulse. The two pulses are centered at $t = 0$ and $t = 0.5$ in units of the vibrational period (300 fs). The change in population on the different eigenvalues is shown as a function of time.

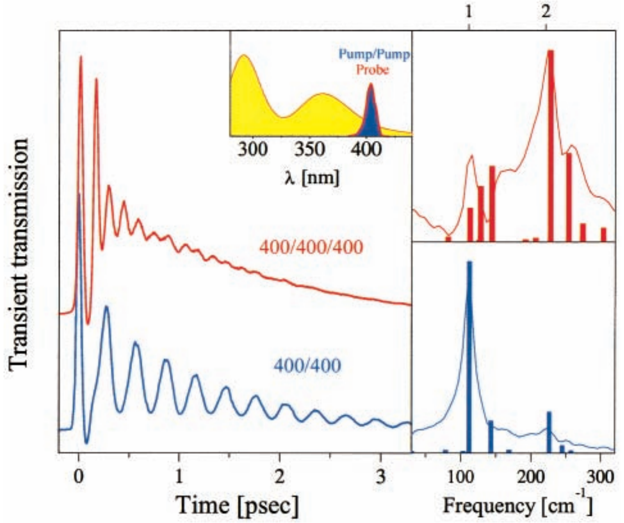

Figure 10. Pump probe signal for I_3^- in ethanol. The figure compares a pump at 400 nm (bottom trace) to a multipump pulse with a time delay of half a period (top trace). The probe is also at 400 nm.

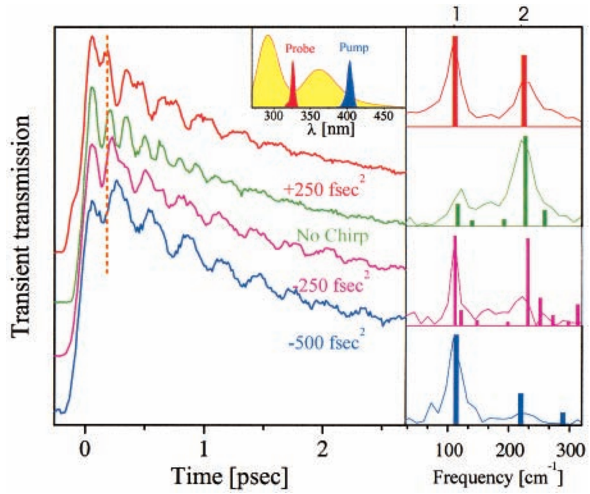

Figure 11. Pump probe signal for I_3^- in acetonitrile for different chirps. The figure compares a pump at 400 nm and a probe at 325 nm with different chirp rates. The vertical line emphasizes the correlation between the phase shift of the signal and the chirp.

8. Again the phase space distribution has a nonclassical component resembling a squeezed state. The symmetric shape of the hole will lead to a dominant second harmonic component irrespective of the detection scheme. This effect can be seen in the experimental results of Figure 10.

D. Chirping the Probe Pulse. Pump 400 nm, Chirped Probe at 325 nm. As stated in section II.C, residual chirp in the probe radiation will break the symmetry of the window function with respect to the zero of momentum and, accordingly, will corrupt the intended C_2 symmetry. In this case study, we will demonstrate this effect and highlight the utility which it provides for pinpointing the coordinates of an evolving ground-state density in phase space. The effective suppression of fundamental modulations as expected for 325 nm probing is demonstrated in the no-chirp trace of Figure 11.

A positive chirp of the probe pulse moves the detection window in the direction of negative momentum (see section II.C and Figure 3). The breaking of the C_2 symmetry will cause the appearance of the first harmonic component in the signal. The same should be true for a negatively chirped probe with the difference that the detection window is shifted to positive momentum. This difference in the direction of the symmetry breaking should cause exactly a π shift in the phase of the first harmonic component irrespective of the amount of chirp. This fact is clearly observed in Figure 11 where, because of the faster relaxation of the second harmonic component, the signal, after sufficient time (~1500 fs), is almost exclusively composed from the first harmonic component. The positive and negative chirped modulations are exactly out of phase. The influence of chirping the probe on the phase of the second harmonic component is gradual and is caused by the shift in the window position to

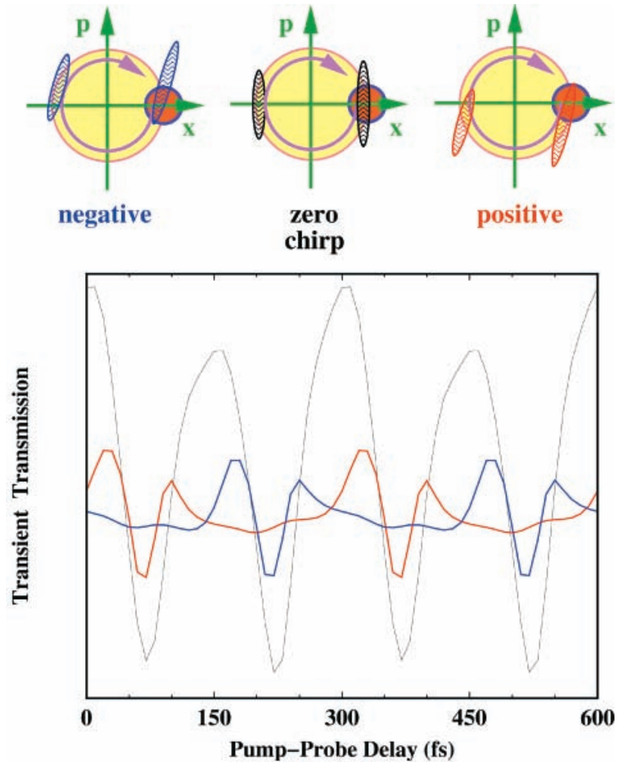

Figure 12. Top: schematic view in phase space of the position of a hole located at the outer turning point and of the observation widows. A positive chirp of the probe shifts the window to the negative momentum direction and also correlates the position and momentum which is observed as a tilt to the window. The opposite is true for the negative chirp. The lower panel shows a simulated pump–probe signal without dissipation. A positive chirp (red) delays the observation of the first window and advances the observation of the second window located at the inner turning point. The tilting causes additional asymmetry between the two observation windows. The negative chirped case is shown in blue and the zero chirp in black.

earlier or later times depending on whether the chirp is positive or negative, cf. Figures 11 and 12.

The lower panel of Figure 12 shows a signal directly simulated for a positive, zero, and negative chirped probe. The simulation was carried out by a direct integration of the Schrödinger equation including the pump and probe fields explicitly. The signal was calculated by adding the Boltzmann weighted signal from each initial ground surface eigenstate. The exact π phase shift between the first harmonic components is clearly evident. The two peaks in the signal are due to the detection by the two observation windows. Their lack of equivalence is the result of a different slope of the difference potential in the right and left observation windows.

Another effect of the chirped probe is to reduce the signal of the late detection in the positively chirped probe and the early detection in the negatively chirped probe. This phenomena is caused by a correlation between momentum and position which tilts the observation windows, cf. Figure 12 and subsection II.C. The tilting means that the probe can follow the motion of the wave packet for a longer time when it is contracting from the outer turning point and that a positive chirp will shift the observation to negative momentum. The tilt in the observation window is the result of a quadratic term $(d^2\Delta/dx^2)_{\Delta=0}$ in the difference potential which causes position momentum correlation. When the simulated signal is compared to the observed one, it is evident that the second derivative of the difference potential is larger in the simulation than in the real I_3^- potentials.

Chirping a probe with a frequency of 364 nm and a pump at 364 also showed a suppression of the second harmonic component. The 364 nm chirped signal differs from the 325 nm chirped signal in that the fundamental component was not enhanced, probably because of its absence from the initial state.

V. Spectral Analysis

The control insight demonstrated in the case studies, in particular the ability to suppress the strongest spectral feature, the fundamental symmetric stretch signal, enables the study of the transient spectroscopy on the ground electronic surface of I_3^- with enhanced precision. With these tools at hand the dephasing dynamics of the different harmonic components composing the signal can be unraveled for different solvents. Moreover weak spectral features such as the antisymmetric stretch and combination band can also be observed. The case studies presented in the previous section are only a small fraction of the data sets which were studied experimentally for I_3^- in ethanol and acetonitrile. Detailed analysis of all of the collected data is presented below in tabulated form.

A. Dephasing Dynamics of the Fundamental and Second Harmonic Symmetric Stretch. Table 1 summarizes the result of the filter-diagonalization analysis of the symmetric stretch dynamics which fit the formula

$$S(t) = \sum_j |d_j| \sin(\phi_j - \omega_j t) e^{-t/\tau_j} \tag{5.1}$$

The amplitude in the table represents the fraction of a particular Fourier component in the total transient signal after the background has been subtracted. A small amplitude of a particular component degraded the reliability of the extracted parameters. When the decay of the second harmonic dynamics was analyzed, the possibility of an inertial effect was checked. A Gaussian fit model was tried for the decay curves but was inferior to the exponential fit.

The main observations in the table concerning the fundamental frequency of the symmetric stretch are the following:

(1) The frequency of the motion is 112 ± 1 cm^{-1} irrespective of the solvent.

(2) The decay is exponential with a decay lifetime of 1030 ± 20 ps for acetonitrile and 950 ± 20 ps for ethanol.

The fundamental frequency in gas phase is very similar, 112 ± 1 cm^{-1},[67] and fits well the ab initio result 114 cm^{-1}.[85] The decay rate is independent of the pump and probe characteristics except when the pump and probe wavelength is close to the middle of the absorption band (∼364 and ∼290 nm) where a very fast decay time is observed. Under these conditions the first harmonic component is suppressed though not entirely. The experiment at 290 nm at the peak of the higher absorption band was done to prove that the RISRS signal is a true ground-state property independent of the excitation frequency. The similarities of the observations at 364 and 390 nm rule out excited-state dynamics and chemical modulation of the nascent product I_2^- as a source of the transient signal. The main observations concerning the second harmonic are as follows:

(1) The frequency of the motion is 224 ± 2 cm^{-1} irrespective of the solvent.

(2) The decay is exponential, with a decay lifetime of 480 ± 50 fs for acetonitrile. Ethanol is slightly slower, 500 ± 50 fs, but it is within the experimental error bars.

(3) Within the experimental error, the decay rate was found to be independent of the initial conditions induced by the pump characteristics.

(4) An exponential decay describes the results well.

TABLE 1: Filter-Diagonalization Fit to the Symmetric Stretch Frequency and Its Second Harmonic

pump [nm]	probe [nm]	solvent	frequency ω [cm^{-1}]	decay τ [fs]	amplitude $\|d\|$	phase ϕ [rad]
290	289	acetonitrile	111 ± 1	620 ± 100	0.4 ± 0.1	1.8 ± 0.2
			229 ± 1	420 ± 50	0.6 ± 0.1	2.3 ± 0.2
287	291	acetonitrile	112 ± 1	650 ± 100	0.6 ± 0.1	2.0 ± 0.2
			227 ± 1	500 ± 50	0.4 ± 0.1	2.4 ± 0.2
364	364	ethanol	112 ± 5	770 ± 40	0.16 ± 0.04	2.1 ± 0.2
			225 ± 5	500 ± 50	0.5 ± 0.1	1.9 ± 0.2
		acetonitrile	113 ± 1	680 ± 100	0.3 ± 0.1	1.7 ± 0.4
			227 ± 1	450 ± 50	0.7 ± 0.1	1. ± 0.2
364 low intensity	400	ethanol	113 ± 3	1200 ± 80	0.1 ± 0.1	0. ± 0.3
			224 ± 1	500 ± 20	0.5 ± 0.1	−1.0 ± 0.1
		acetonitrile	112 ± 2	850 ± 50	0.2 ± 0.1	2.5 ± 0.1
			226 ± 2	460 ± 50	0.8 ± 0.1	−1.1 ± 0.3
364 medium intensity	400	ethanol	112 ± 1	1050 ± 30	0.39 ± 0.02	−0.4 ± 0.3
			222 ± 1	420 ± 70	0.44 ± 0.02	−0.4 ± 0.3
	400	acetonitrile	113 ± 1	1100 ± 60	0.32 ± 0.06	−0.3 ± 0.3
			225 ± 3	400 ± 80	0.68 ± 0.06	−0.8 ± 0.3
364 high intensity	400	ethanol	111 ± 1	1100 ± 80	0.60 ± 0.1	0. ± 0.3
			224 ± 2	520 ± 70	0.3 ± 0.1	−0.6 ± 0.3
		acetonitrile	113 ± 1	1060 ± 30	0.85 ± 0.02	0.5 ± 0.1
			227 ± 2	540 ± 60	0.15 ± 0.02	−0.2 ± 0.1
325	325	ethanol	112 ± 1	1000 ± 200	0.3 ± 0.1	1.7 ± 0.4
			224 ± 1	530 ± 80	0.5 ± 0.1	2.3 ± 0.4
		acetonitrile	113 ± 1	850 ± 100	0.3 ± 0.1	0.2 ± 0.2
			225 ± 1	490 ± 30	0.7 ± 0.1	1.0 ± 0.2
325	400	ethanol	112 ± 1	1040 ± 10	0.7 ± 0.1	
			226 ± 2	430 ± 40	0.14 ± 0.02	
		acetonitrile	113 ± 1	1040 ± 20	0.7 ± 0.1	
			226 ± 2	510 ± 20	0.2 ± 0.1	
400	325 no chirp	acetonitrile	112 ± 1	1300 ± 200	0.2 ± 0.1	−0.2 ± 0.1
			226 ± 3	490 ± 50	0.8 ± 0.1	−3.3 ± 0.1
	325 + chirp		112 ± 1	1000 ± 200	0.8 ± 0.1	−0.3 ± 0.02
			225 ± 2	600 ± 50	0.2 ± 0.1	−1.4 ± 0.2
	325 − chirp		112 ± 1	1100 ± 100	0.6 ± 0.1	2.5 ± 0.3
			226 ± 2	470 ± 50	0.4 ± 0.1	2.4 ± 0.3
400	400	ethanol	112 ± 1	1030 ± 30	0.7 ± 0.1	1.1 ± 0.1
			225 ± 1	480 ± 100	0.2 ± 0.1	1.2 ± 0.2
		acetonitrile	112 ± 1	1100 ± 50	0.6 ± 0.1	1.0 ± 0.2
			225 ± 2	360 ± 50	0.4 ± 0.1	1.1 ± 0.2
400/400	400	ethanol	111 ± 3	1100 ± 100	0.1 ± 0.1	0.0 ± 0.2
			226 ± 1	480 ± 50	0.6 ± 0.1	0.9 ± 0.2
		acetonitrile	113 ± 2	1040 ± 60	0.1 ± 0.1	1.9 ± 0.2
			226 ± 2	410 ± 50	0.9 ± 0.1	0.6 ± 0.2

TABLE 2: Filter-Diagonalization Fit to the Antisymmetric Stretch Frequency and Combination Band

pump [nm]	probe [nm]	solvent	frequency ω [cm^{-1}]	decay τ [fs]	amplitude |d|
364H	400	ethanol	142 ± 5	720 ± 70	0.15 ± 0.02
325	325	ethanol	148 ± 5	650 ± 300	0.13 ± 0.07
400	325	ethanol	147 ± 2	670 ± 50	0.08 ± 0.03
400	325	ethanol	263 ± 2	364 ± 50	0.1 ± 0.03
400	325C	ethanol	144 ± 2	680 ± 50	0.11 ± 0.03
400	325C	ethanol	253 ± 2	870 ± 50	0.11 ± 0.03
400/400	400	ethanol	143 ± 3	700 ± 100	0.12 ± 0.03
400/400	400	ethanol	255 ± 3	350 ± 100	0.2 ± 0.03

B. Dephasing Dynamics of the Antisymmetric Stretch and the Combination Band. Table 2 shows the result of filter-diagonalization analysis for the antisymmetric stretch and combination band dynamics. A significant signal could only be detected in ethanol. Suppressing the fundamental frequency unravels the weak signals of other frequencies.

(1) The frequency of the antisymmetric stretch is 143 ± 2 cm^{-1}.

(2) The decay is exponential, with a decay lifetime of 640 ± 50 fs.

(3) The frequency of the combination band is 253 ± 2 cm^{-1}.

(4) The decay is exponential, with a decay lifetime of 480 ± 70 fs.

(5) The decay of the combination band is slower than the expected decay corresponding to the sum of the rates of the symmetric and antisymmetric stretch (400 fs).

An antisymmetric stretch frequency of 140 cm^{-1} for I_3^- in ethanol was inferred by Kühne et al.[53] Ab initio calculations indicate a frequency of 147 cm^{-1} (see ref 85).

VI. Discussion

Impulsive coherent control of molecular dynamics hinges on a separation of time scales between the light induced transitions and the intramolecular vibrational motions when impulsive conditions prevail. It is particularly attractive for general control of ground electronic surface dynamics in condensed phases. The brevity of the control process allows initiation of particular modes of motion before dissipative forces take over.

One may ask whether this process is coherent control? The accepted criterion is that coherent control is an *interference* effect with at least two pathways leading to the final result.[30,55,56] Reconsidering the process that creates the dynamical hole, it is clear that cycling of the amplitude through the excited electronic surface and its *interference* with the initial ground-state wave function is the main source of control. The basic mechanism of coherent control is supplemented by multipulsing which allows further interference pathways.

Many goals have been envisioned for coherent control, from the photosynthesis of exotic molecules to precisely timed switching of currents in mini-scale electronic devices. Here we seek more fundamental insights. On the one hand, to understand how parameters of the excitation field influence the induced dynamics in the triiodide ground state; on the other hand, to employ the degrees of control provided by the explored parameters to learn more about the mechanisms governing vibrational relaxation of triiodide in various solvents.

Impulsive optical excitation, our vehicle of control, is by no means a new topic.[1,7,9,13,15,57,58] However, as demonstrated in the present study, new insights concerning this process, both of fundamental and applied importance, are still being uncovered. The widespread application of impulsive photoexcitation, with femtosecond lasers in recent years, underlines the importance of understanding its finer details, even in the limited scope of induced ground state dynamics. Indeed, the material systems of relevance extend beyond the molecular, identified in the Introduction. Phonons which dress optical transitions in solids,[54] acoustical phonons in nanoclusters,[59] charge transfer reactions,[60] or photoassociation of cold atoms[61] can replace the vibrational coordinates in this scenario. Although the frequencies of the induced coherences may vary widely, the underlying principles are essentially the same.

One fundamentally significant finding in the present study is the striking demonstration of the inadequacy of a perturbative approach for describing impulsively induced ground state vibrational dynamics and its spectroscopic signature. The lowest power in field intensity for a ground state variation should be quadratic. Yet, here it was demonstrated that the asymptotic dependence of the momentum change on intensity was linear. Equally significant is the nearly perfect agreement, both in form and in the levels of excitation, between the experiments and the theoretical approach chosen here. In this study, an alternative approach is used to simulate the material response to irradiation, using direct propagation methods of the molecular density matrix. A similar approach has recently been suggested for simulating signals of CARS experiments and of other four-wave mixing spectroscopies.[62−65] These points are particularly significant because many of the alternative theoretical descriptions dealing with this process are cast in terms of the perturbation theory, and must therefore be suspected of glossing over the limitations of this approach as demonstrated in the current results.

One of the main sources of insight is the phase space picture of the dynamical hole. With this tool we are able to rationalize the control manipulations. Creating a state with C_2 symmetry in phase space will completely eliminate the fundamental frequency from the signal. Three different techniques were demonstrated in the case studies to induce such a symmetry. Breaking this symmetry is the agent of control. It can be done either in the momentum direction by varying the intensity or in the coordinate direction by tuning the pump wavelength. A combination of these two control levers can induce dynamics with a controlled combination of amplitude and phase of the first and second harmonics of the signal. Chirping the pump, which was not demonstrated explicitly, would add the ability to move in the diagonal direction in phase space. There exist other sources of uncontrolled symmetry breaking such as anharmonicity. These can be included or neutralized by the active control knobs. The symmetry in phase space is also the key to understanding the probe manipulation. We have elaborated on the concept of a window function. The window function can be thought of as a shaped porthole limiting the views of phase space. By constructing a window with C_2 symmetry properties only patterns with such a symmetry are observed in the signal.

The effects of spectral chirp in the pump and probe pulses are intriguing. Although up to this point we have related to this parameter on equal footing with the others tested, in reality, the effects of pump and probe chirp were stumbled over more than they were intentionally recorded. For 400 pump and 325 probe data, we found it hard to reproduce results, until full chirp scans were conducted! This fact, more than any other, exemplifies just how sensitive the reported results are to slight residual spectral chirp in the pump and probe pulses. In other words, residual chirp which had negligible effects in other wavelength combinations strongly influenced the results of these pump probe schemes. In retrospect, this effect can be rationalized and even used to our advantage in understanding the underlying dynamics. Accordingly, the quantum motion of the induced hole is followed in phase space in analogy with the scheme suggested by Zadoyan et al.[32] for following excited state wave packet evolution. Nonetheless, our results serve as a reminder of just how strongly residual chirp can effect the RISRS signals under specific conditions when short and therefore broadband pulses are being employed.

Our results are also illuminating from an applied point of view. RISRS has been previously used as a spectroscopic method, both by ourselves[10,18] and by others.[6,25,52,59,66−68] Its natural aptness for recovering vibrational dynamics of low frequency modes stems from the fact that it is a time resolved method. Here we have not only recovered accurate vibrational dynamics pertaining to first-order coherences but also obtained similar data for one higher harmonic. Furthermore, the possibility of first harmonic suppression by the various methods described allows the determination of decay dynamics for the second harmonic and for weaker bands such as the antisymmetric stretch fundamental in ethanol with much higher precision.

Whereas all of the observed modulations have been adequately modeled assuming exponential dephasing, it is important to point out that any deviations from exponential decays, as in cases of intermediate to slow modulation limits in a Kubo line shape scenario, could be detected using this spectroscopy as well. However, the methods discussed above do not require any assumptions or functional representations of the prominent fundamental modulation decay in order to implement its very effective suppression, allowing reliable and much closer scrutiny of the weaker modulation features. In contrast, an arithmetic subtraction for achieving the same result would require representation of the fundamental frequency component, perhaps, as a Lorentzian peak in frequency, or an exponentially decaying oscillation in time. Although it might fit the real feature very well near its center, it could equally deviate substantially on the wings distorting the structure of the low intensity features whose extraction was the objective in the first place. This is a unique capability of impulsive Raman, and no counterpart exists for equivalent frequency domain spectroscopies. Accordingly, it might find applications even in cases where the inherent time resolution of this method is of no consequence.

The triiodide ion is a prime example for the utility of RISRS as an applied spectroscopic method. Above, the information provided by this spectroscopy concerning the ground state vibrational dynamics of I_3^- in solution has been outlined. Other spectroscopic methods that provide similar relaxation parameters are the resonance Raman and CARS methods. The later is irrelevant in the triiodide case, because the dephasing times and the vibrational period are of the same order of magnitude. Resonance Raman spectra of triiodide have been collected and analyzed by Myers and co-workers.[23,24,69] However, the line widths which best fit the data are nearly two times broader than predicted by the dephasing times extracted from our data. A priori this discrepancy does not necessarily identify which method is providing the more accurate result. However, the dephasing times measured match up favorably with line widths appearing in preresonant Raman spectra. An exception in the RISRS data was found when the pump and probe were positioned at the peak of the absorption band the first harmonic was found to decay more rapidly. This may indicate a possible sensitivity of the decay time to the shape of the dynamical hole. Further investigation in this direction is in progress. In view of the close agreement of our data with the preresonant Raman line widths, we conclude that it provides a more precise measure of ground-state vibrational dynamics of fundamentals and higher harmonics of I_3^-.

Along with the advantages elaborated upon above, the RISRS technique also suffers from substantial limitations. As in the case of resonance Raman spectroscopy, spectral interference from long-lived excited state populations can mask the ground state dynamics, or at least superimpose spectral modulations from ground state coherences with others related to wave packet motions in the excited state.[78,79] Even in the I_3^- case, where dissociation rapidly dissipates the excited-state density, there exists the possibility of interference from spectral modulations in the I_2^- product, because of its UV absorption band which is centered at ~364 nm in relaxed diiodide. To test this possibility, we duplicated a number of experiments which were originally conducted using the lower excited state ($\lambda_{\max} = 364$ nm), on the intense absorption band centered at 292 nm. The lack of significant differences in the results proves that contribution to the signal from chemical modulations caused by coherent vibrations of the product I_2^-, which partly overlaps the lower absorption band, are absent.

The analysis of the RISRS signals corroborates previous measurements of the fundamental frequencies of I_3^- in the solvents tested.[10,23,24,70−72] Compared to isolated gas-phase I_3^-, very small solvent shifts are observed for the symmetric stretch mode.[66] The measured frequencies agree very well with ab initio calculations on isolated[50] I_3^-, which again indicates small solvent shifts. The weak influence of the solvent is remarkable in view of the strong interactions existing between the negatively charged molecular ion and the surrounding solvent. The central frequencies of the electronic transitions are also negligibly influenced by solvation. Indeed a recent study by Choi et al.[22] shows that the central frequencies in the gas phase are identical to the ones in polar solvents.

The results related above not only scrutinize the process of impulsive excitation itself but reveal the mechanisms of vibrational relaxation active in the triiodide ground state. In a previous RISRS study of I_3^- in cooled ethanol solutions, dephasing dynamics were analyzed using the Kubo line shape theory.[73−75] To do so, the dephasing contribution made by population relaxation is estimated. In ethanol solutions, both our own results[76] and those of others[77] demonstrated that T_1(vib) for the symmetric stretch at low excess vibrational energies is between 3 and 4 ps at room temperature, and remains in that range all of the way down to 100 K. A similar time scale was also found for acetonitrile solutions at room temperature. Given these values for the rate of population relaxation, and that $1/T_2 = 1/T_2^* + 1/2T_1(\text{vib})$, with T_2^* representing the pure dephasing time, we find that the T_1 process makes only a minor contribution to the dephasing of the symmetric stretching mode of I_3^- in either solvent. Thus, pure dephasing must be the primary mechanism leading to the loss of coherence in this mode of vibration.

As stated above, an exponential model fits the dephasing dynamics of both the fundamental and the second harmonic of the symmetric stretching motions observed in ethanol and acetonitrile. The second harmonic decays about 2.3 times faster than the fundamental. Within the Kubo line shape formalism, the exponential dephasing dynamics indicates that the medium induced spectral modulations are in the fast modulation limit. Accordingly, the inverse spread of momentary frequencies, $1/\Delta\omega$, must be substantially longer than the time scale for stochastic changes of the frequency τ_c. In terms of these parameters, Kubo line shape theory[80] provides the following value of the dephasing time of the fundamental $-T_2^* = 1/(\Delta\omega^2\tau_c)$. The same stochastic frequency fluctuations which give rise to dephasing of the fundamental must also be those which kill the phase memory in the second harmonic as well; thus, τ_c is identical for both. In contrast, the spread of the frequencies for the second harmonic is twice as broad, and within this framework, it is expected that the dephasing time for the second harmonic would be four times as rapid. Within this analysis, a subquadratic ν dependence of dephasing times is possible, but only in the intermediate to slow modulation regimes, where the phase memory is markedly nonexponential, contrary to our result.

Nonquadratic ν dependence of dephasing rates such as that observed here is not limited to the triiodide ion and has been observed using other methods in a variety of molecular systems in solution.[81] These observations have led to active recent theoretical debate concerning the underlying mechanisms for dephasing.[80]

The exponential decay of the signals suggests that a semigroup memoryless approach is sufficient to describe the observations. In the past, a quantum Gaussian semigroup model has been used to describe the dephasing.[10] The model is an alternative description of the fast modulation limit of the Kubo line shape theory where the dephasing is caused by fast and abundant frequency modulation induced by the solvent. The Gaussian semigroup model also predicts quadratic ν dependence which is inconsistent with the observations. Latter we have suggested an alternative Poisson dephasing mechanism,[15] which carries the view of isolated abrupt disruptions to the vibrational dynamics. If the disruption causes a large phase shift, the model can explain subquadratic ν dependence. This viewpoint is consistent with a recent study by Yamaguchi, who suggested describing the dephasing dynamics by a binary collision model.[82] The model originated in describing gas phase dephasing caused by isolated elastic collisions from other gas particles.[83] The basic assumption is that each collision event is random and uncorrelated; therefore, the process is the quantum analogue of a Poisson process.[84] Yamagauchi applies the model to the condensed phase environment on the basis of an analysis of a large set of data from different molecules and solvents showing that subquadratic ν dependence is quite universal. A direct simulation for the dissipative dynamics of the I_3^- system by solving the Liouville von Neumann equation with a Poisson dephasing model is in progress. We are currently investigating the appropriate model for describing the dephasing dynamics of I_3^- by measuring the decay of high harmonics at reduced temperatures. Thus, finally our combined efforts in experiment and theory have come full cycle: starting out to characterize elementary light induced processes and ultimately opening the door for appreciating fundamental aspect of vibrational dephasing dynamics in polar solvents.

VII. Conclusions

The comprehensive study of the RISRS process for the I_3^- molecular ion has resulted in a wealth of insight into elementary light−matter interactions in condensed phases. The main points are highlighted as follows:

(1) Experimental demonstration of coherent control of ground-state dynamics which enables suppression of the fundamental component or control of the amplitude and phase of the first and second harmonic components in the transient signal.

(2) Theoretical analysis in phase space, in particular the identification of the importance of C_2 symmetry of the density in phase space is able to rationalize the control manipulations.

(3) Experimental sensitivity to intensity and chirp necessitate a theoretical foundation which goes beyond perturbation theory. The nonperturbative coordinate dependent two-level system supplies a conceptual picture verified by experiment and simulation.

(4) The suppression of the first harmonic provides for the first time an accurate measure of dephasing dynamics for the second harmonic symmetric stretching and other weak spectral features in I_3^-.

(5) The dynamics and decay times of dephasing for the first and second symmetric stretching harmonics contradict the predictions of Kubo line shape theory. This is significant not only because it points to shortcomings of a formalism which is widely accepted for describing vibrational phase relaxation but also because similar cumulant expansions of correlation functions are fundamental components in universally accepted frameworks for analysis of nonlinear optical spectroscopies.

Our accumulated knowledge concerning the I_3^- reactant in solution, has been a crucial ingredient in appreciating the capabilities of the RISRS technique as a useful alternative to frequency domain vibrational spectroscopies. It has served to demonstrate that this molecule is taking its place as a valuable model liquid-phase reactive system.

Acknowledgment. We thank H. C. Kapteyn, M. Murnane, R. M. Hochstrasser and K. Wynne, for helpful suggestions concerning the laser system. E. Mastov has given valuable technical assistance. We thank D. Neuhauser and V. Mandelshtam for helping to implement the filter diagonalization analysis. We thank D. Neumark for fruitful discussions and the sharing of unpublished data. This research was supported by the Israel Science Foundation (Moked) administered by the Israel Academy of Science. The Fritz Haber and Farkas Research Centers are supported by the Minerva Gesellschaft für die Forschung, GmbH München, FRG.

References and Notes

(1) Dhar, L.; Rogeres, J. A.; Nelson, K. A. *Chem. Rev.* **1994**, *94*, 157.

(2) Zewail, A. H. *J. Phys. Chem. A* **2000**, *104*, 5660.

(3) Chesnoy, J.; Mokhtari, A. *Phys. Rev. A* **1988**, *38*, 3566.

(4) Wise, F.; Rosker, M. J.; Tang, C. L. *J. Chem. Phys.* **1987**, *86*, 2827.

(5) Hartke, B.; Kosloff, R.; Ruhman, S. *Chem. Phys. Lett.* **1989**, *158*, 238.

(6) Dexheimer, S. L.; Wang, Q.; Peteanu, L. A.; Pollard, W. T.; Mathies, R. A.; Shank, C. V. *Chem. Phys. Lett.* **1992**, *188*, 61.

(7) Pollard, W. T.; Mathies, R. A. *Annu. Rev. Phys. Chem.* **1992**, *43*, 497.

(8) Baumert, T.; Gerber, G. *Phys. Scripta* **1997**, *T72*, 53.

(9) Mukamel, S. *Principles of Nonlinear Optical Spectroscopy*; Oxford University Press: New York, 1995.

(10) Banin, U.; Bartana, A.; Ruhman, S.; Kosloff, R. *J. Chem. Phys.* **1994**, *101*, 8461.

(11) Bartana, A.; Banin, U.; Ruhman, S.; Kosloff, R. *Chem. Phys. Lett.* **1994**, *229*, 211.

(12) Baumert, T.; Engel, T.; Meier, C.; Gerber, G. *Chem. Phys. Lett.* **1992**, *200*, 488.

(13) Ungar, L. W.; Cina, J. A. *J. Lumin.* **1994**, *63*, 345.

(14) Ungar, L. W.; Cina, J. A. *Adv. Chem. Phys.* **1997**, *100*, 171.

(15) Ashkenazi, G.; Banin, U.; Bartana, A.; Kosloff, R.; Ruhman, S. *Adv. Chem. Phys.* **1997**, *100*, 229.

(16) Banin, U.; Ruhman, S. *J. Chem. Phys.* **1993**, *98*, 4391.

(17) Banin, U.; Kosloff, R.; Ruhman, S. *Israel. J. Chem.* **1993**, *33*, 141.

(18) Banin, U.; Kosloff, R.; Ruhman, S. *Ultrafast Phenomena IX*, **1994**, 68.

(19) Gershgoren, E.; Banin, U.; Ruhman, S. *J. Phys. Chem.* **1998**, *102*, 9.

(20) Awtrey, A. D.; Connick, R. E. *J. Am. Chem. Soc.* **1951**, *73*, 1842.

(21) Pimentel, G. C. *J. Chem. Phys.* **1951**, *19*, 446.

(22) Choi, H.; Bise, R. T.; Hoops, A. A.; Neumark, D. *J. Chem. Phys.* **2000**, *113*.

(23) Johnson, A. E.; Myers, A. B. *J. Chem. Phys.* **1995**, *102*, 3519.

(24) Johnson, A. E.; Myers, A. B. *J. Phys. Chem.* **1996**, *100*, 7778.

(25) Kühne, T.; Vöhringer, P. *J. Chem. Phys.* **1996**, *105*, 10788.

(26) Jonas, D. M.; Bradforth, S. E.; Passino, S. A.; Fleming, G. R. *J. Phys. Chem.* **1995**, *99*, 2594.

(27) Ruhman, S.; Kosloff, R. *J. Opt. Soc. Am. B* **1990**, *7*, 1748−1752.

(28) Bardeen, C. J.; Wang, Q.; Shank, C. V. *Phys. Rev. Lett.* **1995**, *75*, 3410.

(29) Bardeen, C. J.; Wang, Q.; Shank, C. V. *J. Phys. Chem.* **1998**, *A 102*, 2759.

(30) Rice, S. A.; Zhao, M. *Optical Control of Molecular Dynamics*; John Wiley and Sons: New York, 2000.

(31) Hiller, E. M.; Cina, J. A. *J. Chem. Phys.* **1996**, *105*, 3419.

(32) Zadoyan, R.; Schwentner, N.; Apkarian, V. A. *Chem. Phys. Lett.* **1998**, *233*, 353.

(33) Cao, J.; Bardeen, C. J.; Wilson, K. R. *Phys. Rev. Lett.* **1998**, *80*, 1406.

(34) Allen, L.; Eberly, J. H. *Optical Resonance and Two-Level Atoms*; Dover Publications: New York, 1987.

(35) Sawicki, D.; Eberly, J. H. *Opt. Express* **1999**, *4*, 217. http//www.opticsexpress.org/oearchive/source/9096.htm.

(36) Vala, J.; Kosloff, R. *Opt. Express* **2001**, *8*, 238. http//www.opticsexpress.org/

(37) Tal Ezer, H.; Kosloff, R. *J. Chem. Phys.* **1984**, *81*, 3967.

(38) Wigner, E. P. *Phys. Rev.* **1932**, *40*, 749.

(39) Hillery, M.; O'Connel, R. F.; Scully, M. O.; Wigner, E. P. *Phys. Rep.* **1984**, *106*, 121.

(40) Asaki, M. T.; Huang, C. P.; Garvey, D.; Zhou, J.; Kapteyn, H. C.; Murnane, M. *Optics Lett.* **1995**, *18*, 977.

(41) Backus, S.; Peatross, J.; Huang, C. P.; Murnane, M.; Kapteyn, H. C. *Optics Lett.* **1995**, *20*, 2000.

(42) *Labview*, version 5; National Instruments 1998.

(43) Wall, M. R.; Neuhauser, D. *J. Chem. Phys.* **1995**, *102*, 8011.

(44) Pang, J. W.; Dieckmann, T.; Feigon, J.; Neuhauser, D. *J. Chem. Phys.* **1998**, *108*, 8360.

(45) Mandelshtam, V. A. *J. Chem. Phys.* **1998**, *108*, 9999.

(46) Lindenberger, F.; Stockl, R.; Asthana, B. P.; Laubereau, A. *J. Phys. Chem.* **1999**, *103*, 5655.

(47) Vöringer, P.; Scherer, N. F. *J. Phys. Chem.* **1995**, *99*, 2684.

(48) Chen, J. H.; Mandelshtam, V. A. *J. Chem. Phys.* **2000**, *112*, 4429.

(49) Nelson, K. A.; Dwayne Miller, R. J.; Lutz, D. R.; Fayer, M. D. *J. Appl. Phys.* **1982**, *53*, 1144.

(50) Lynden-Bell, R. M.; Kosloff, R.; Ruhman, S.; Danovich, D.; Vala, J. *J. Chem. Phys.* **1998**, *109*, 9928.

(51) Garrett, G. A.; Rojo, A. G.; Sood, A. K.; Whitaker, J. F.; Merlin, R. *Science* **1997**, *275*, 1638.

(52) Kumar, A. T. N.; Rosca, F.; Widom, A.; Champion, P. M. *J. Chem. Phys.* **2001**, *114*, 701.

(53) Kühne, T.; Küster, R.; Vöhringer, P. *Chem. Phys.* **1998**, *233*, 161.

(54) Bammel, K.; Dietrich, P.; Schwentner, N. *J. Chem. Phys.* **1999**, *111*, 2123.

(55) Rice, S. *Science* **1992**, *258*, 412.

(56) Brumer, P.; Shapiro, M. *Annu. Rev. Phys. Chem.* **1992**, *43*, 257.

(57) Kleinman, V. D.; Arrivo, S. M.; Melinger, J. S.; Heilweil, E. J. *Chem. Phys.* **1998**, *233*, 207.

(58) Heid, M.; Chen, T.; Pausch, R.; Schwoerer, H.; Kiefer, W. *J. Chinese Chem. Soc.* **2000**, *47*, 637.

(59) Cerullo, G.; De Silvestri, S.; Banin, U. *Phys. Rev. B* **1999**, *60*, 1928.

(60) Kambhampati, P.; Son, D. H.; Kee, T. W.; Barbara, P. F. *J. Phys. Chem.* **2000**, *104*, 10637.

(61) Vala, J.; Dulieu, O.; Masnou-Seeuws, F.; Pillet, P.; Kosloff, R. *Phys. Rev.* **2001**, *A63*, 013412.

(62) Meyer, S.; Engel, V. *J. Raman. Spec* **2000**, *31*, 33.

(63) Ebeland, G.; Shinke, R. *J. Chem. Phys.* **1994**, *101*, 1865.

(64) Stock, G.; Domcke, W. *Phys. Rev.* **1992**, *A45*, 3032.

(65) Shen, Y. C.; Cina, J. A. *J. Chem. Phys.* **1999**, *110*, 9793.

(66) Greenblatt, B. J.; Zanni, M. T.; Neumark, D. M. *Chem. Phys. Lett.* **1996**, *258*, 523.

(67) Zanni, M. T.; Taylor, Greenblatt, B. J.; Soep, B.; Neumark, D. M. *J. Chem. Phys.* **1996**, *107*, 7613.

(68) Rosca, F. A. T.; Kumar, N.; Ye, X.; Sjodin, T.; Demidov, A. A.; Champion, P. M. *J. Phys. Chem.* **2000**, *A 104*, 4280.

(69) Ashkenazi, G.; Kosloff, R.; Ruhman, S.; Tal-Ezer, H. *J. Chem. Phys.* **1995**, *103*, 10005.

(70) Kiefer, W.; Bernstein, H. J. *Chem. Phys. Lett.* **1972**, *16*, 5.

(71) Kaya, K.; Mikami, N.; Ito, M. *Chem. Phys. Lett.* **1972**, *16*, 151.

(72) Zanni, M. T.; Davis, A. V.; Frischkom, C.; Elhanine, M.; Neumark, D. M. *J. Chem. Phys.* **2000**, *112*, 88847.

(73) Kubo, R. *Math J. Phys.* **1963**, *4*, 174.

(74) Oxtoby, D. W. *Adv. Chem. Phys.* **1979**, *40*, 1.

(75) Wang, Z. H.; Wasserman, T.; Gershgoren, F.; Ruhman, S. *J. Mol. Liq.* **2000**, *86*, 229.

(76) Wang, Z.; Wasserman, T.; Gershgoren, E.; Vala, J.; Kosloff, R.; Ruhman, S. *Chem. Phys. Lett.* **1999**, *313*, 155−161.

(77) Hess, S. S.; Bursing, H. H.; Vöhringer, P. *J. Chem. Phys.* **1999**, *111*, 5461.

(78) Scherer, N. F.; Jonas, D. M.; Fleming, G. R. *J. Chem. Phys.* **1993**, *99*, 4704.

(79) Baumert, T.; Buhler, B.; Grosser, M.; Thalweiser, R.; Weiss, V.; Weidenmann, E.; Gerber, G. *J. Phys. Chem.* **1991**, *95*, 8103.

(80) Gayathri, N.; Bagchi, B. *Phys. Rev. Lett.* **1999**, *82*, 4851.

(81) Tominaga, K.; Yoshihara, K. *J. Phys. Chem.* **1998**, *A 102*, 4222.

(82) Yamaguchi, T. *J. Chem. Phys.* **2000**, *112*, 8530.

(83) Levine, R. D. *Quantum mechanics of molecular rate processes*; Oxford University Press: New York, 1969.

(84) Lindblad, G. *Commun. Math. Phys.* **1976**, *48*, 119.

(85) Vala, J.; Kosloff, R.; Harvey, J. N. *J. Chem. Phys.* **2001**, *114*, 7413.